

Circular orbits of test particles interacting with massless linear scalar field of the naked singularity

O. S. Stashko^{1,2,3,4} and V. I. Zhdanov^{4,5}

¹Frankfurt Institute for Advanced Studies, Frankfurt am Main, Germany

²Goethe Universität, Max-von-Laue Str. 1, Frankfurt am Main 60438, Germany

³Theoretical Physics Department, CERN, 1211 Geneva 23, Switzerland

⁴Taras Shevchenko National University of Kyiv, Kyiv 01601, Ukraine

⁵Igor Sikorsky Kyiv Polytechnic Institute, Kyiv 03056, Ukraine



(Received 6 September 2022; accepted 20 October 2022; published 28 November 2022)

We study effects of the particles coupling with scalar field (SF) on the distribution of stable circular orbits (SCO) around the naked singularity described by the well-known Fisher-Janis-Newman-Winicour solution (F/JNW). The power-law and exponential models of the particle–SF interaction are analyzed. The focus is on the nonconnected SCO distributions. A method is used that facilitates numerical studies of the SCO regions in the case of the general static spherically symmetric metric. In case of F/JNW, we show that coupling between particles and SF can essentially complicate the topology of the SCO distributions. In particular, it can lead to new nonoverlapping SCO regions, which are separated by unstable orbits and/or by regions where the circular orbits do not exist.

DOI: [10.1103/PhysRevD.106.104049](https://doi.org/10.1103/PhysRevD.106.104049)

I. INTRODUCTION

Static spherically symmetric configurations of general relativity (GR) with the linear massless scalar field (SF) are described by the exact analytic solution of Einstein-SF equations, which was first derived in 1948 by Fisher [1] and later rediscovered in the other coordinates by Janis, Newman and Winicour [2]. We will refer to this solution as F/JNW. Subsequently, Wyman [3] obtained this solution within a more general consideration; see also [4,5] and comments in [6,7]. The F/JNW solution is asymptotically flat, it contains the globally naked singularity (NS) in the center [8], i.e., it can be observed from the infinity. There are analytic generalizations of F/JNW in case of the higher dimensions [7,9] and in case of several linear massless SFs [10].

The picture of the stable circular orbits (SCO) of test bodies in case of F/JNW metric has been first studied by Chowdhury *et al.* [11] who revealed the possibility of nonconnected SCO regions, which are separated by unstable circular orbits (UCO). This is an important feature that distinguishes F/JNW from the case of ordinary Schwarzschild black holes, where there is the region of nonexistence of circular orbits (NECO) near the center,

then the UCO ring and then the outer (unbounded) region of SCO. Images of thin accretion disks related to the circular orbits distributions (COD) in case of F/JNW solutions have been considered in [12,13].

The unusual structure of COD around relativistic objects is not a prerogative of F/JNW; the uncomplete list of papers includes, e.g., [14–24]. As for the configurations with scalar fields, apart from F/JNW, the nonconnected SCO distributions have been demonstrated in the case of massive SF [23] and in case of nonlinear SFs with the monomial potential [10,24]. The above cases mainly deal with NSs, however, the nonconnected SCO distributions can arise in presence of the event horizon as well; see, e.g., [19] dealing with the “Mexican hat” SF potential.

We note that the investigation of COD is an important tool to study strong gravitational fields around compact astrophysical objects, because this is the first step to figure out the properties of real accretion discs and their observational properties. The purpose of such studies is to screen out theories alternative to GR, or, conversely, to look for putative signals of a “new physics” that can be verified in observations. Anyway, investigations of such exotic structures as NSs with unusual accretion disks is interesting at least because they make the standard black hole paradigm falsifiable.

The works [11–24] deal with the geodesic particle motion; no additional particle interaction is introduced. In the present paper we focus on the nonconnected SCO distributions under assumptions that the massive particles interact with SF. Analogous interactions naturally arise in the scalar-tensor theories [25–27] and in the $f(R)$ -gravity

Published by the American Physical Society under the terms of the [Creative Commons Attribution 4.0 International license](https://creativecommons.org/licenses/by/4.0/). Further distribution of this work must maintain attribution to the author(s) and the published article’s title, journal citation, and DOI.

after transition to the Einstein frame (see, e.g., [28,29]). There are hard limitations on the particles–SF interaction imposed by the weak-field gravitational experiments [30]. Nevertheless, NS is a very special object with strong gravitational field and we wonder whether coupling of particles with SF in the vicinity of NS can lead to new observational features that can be used to differentiate between ordinary black hole and NS.

We investigate the effects in the SCO structure due to various couplings of the particles with SF within simple toy models. The particles move in the external gravitational and scalar fields of the F/JNW naked singularity. In Sec. II we write down the basic equations of motion of the particle.

In Sec. III we consider two types of the coupling, which are applied to the equations of the particle motion in the fields of F/JNW solutions. We present here the list of possible distributions of the circular orbits; in particular, we present those, which do not occur in case of usual geodesic motion of the particles. In Sec. IV we discuss the results.

II. BASIC RELATIONS IN CASE OF COUPLING OF PARTICLES WITH SF

We consider the motion of the test particles interacting with SF ϕ in the four dimensional space-time of general relativity endowed with metric $g_{\alpha\beta}$. We assume that the particles have small masses, which makes it possible to neglect the mutual interaction between the particles and their feedback on the gravitational and scalar fields.

For one particle we assume the action¹

$$S_m = -m \int ds \psi(\phi(x)), \quad ds = \sqrt{g_{\alpha\beta}(x) \frac{dx^\alpha}{d\tau} \frac{dx^\beta}{d\tau}} d\tau, \\ x \equiv x(\tau); \quad (1)$$

where trajectory $x(\tau)$ is parametrized by a parameter τ ; $\psi(\phi) = 1 + \xi(\phi)$ is responsible for the interaction of particles with SF. We assume $\psi > 0$ in order to avoid negative masses of the particles. The value ξ is expected to be sufficiently small in the weak-field systems. However, we look for effects of the interaction in the strong field region, where ξ may be comparable to unity.

The aim of this paper is to show that an additional coupling between particles and SF (besides the indirect interaction through the gravitational field depending on SF by means of the Einstein equations) can essentially complicate the topology of the SCO distributions, in addition to complications due to possible introduction of the nonlinear self-interaction SF potentials. This is motivated, in particular, by a number of models, in which the coupling arises after the transition from Jordan to Einstein frame either in the Brans–Dicke theory or in the $f(R)$ -gravity [25–29]. In these cases the interaction with SF is simply a result of the conformal

transformation of the metric; but this leads also to changes of the SF self-interaction. However, in this paper we are looking for potentially interesting qualitative coupling effects apart from those due to the SF potential, which manifest themselves in the strong gravitational field of a naked singularity. There are various ways to introduce the coupling into the particle action, and we see no physical reason to prefer one model over another. In this situation, the way out is to consider a number of examples with different couplings. Some examples will be considered below in Secs. III A and III B. Physically, the coupling may be, e.g., due to some dependence of masses or interaction constants upon SF.

The equations of motion for the massive test particle trajectory as a function of the proper time s obtained from action (1) are

$$\frac{d}{ds} \left(\psi g_{\alpha\beta} \frac{dx^\beta}{ds} \right) = \frac{\partial \psi}{\partial x^\alpha} + \frac{\psi}{2} \frac{\partial g_{\beta\gamma}}{\partial x^\alpha} \frac{dx^\beta}{ds} \frac{dx^\gamma}{ds}, \quad (2)$$

$\psi \equiv \psi[\phi(x(s))]$. Equation (2) is equivalent to the geodesic equation for the conformal metric $\tilde{g}_{\mu\nu} = \psi^2 g_{\mu\nu}$ with the canonical parameter \tilde{s} : $d\tilde{s} = \psi ds$. The trajectories of photons and the other massless particles are the same under the conformal transformation as for $\psi = 1$.

The equivalent (explicitly covariant) form of this equation of motion is

$$\frac{\delta}{ds} \frac{dx^\beta}{ds} = \left(g^{\beta\mu} - \frac{dx^\beta}{ds} \frac{dx^\mu}{ds} \right) \frac{\partial \ln \psi}{\partial x^\mu}, \quad (3)$$

where δ/ds stands for the covariant differentiation (with respect to $g_{\mu\nu}$) along the particle trajectory.

It is easy to check that in virtue of (2) or (3)

$$\frac{d}{ds} \left[\psi^2 \left(g_{\mu\nu} \frac{dx^\mu}{ds} \frac{dx^\nu}{ds} - 1 \right) \right] = 0. \quad (4)$$

This equation is consistent with usual normalization

$$g_{\mu\nu} \frac{dx^\mu}{ds} \frac{dx^\nu}{ds} = 1. \quad (5)$$

Now we move on to the metric of the static spherically symmetric space-time

$$dS^2 = A(r)dt^2 - B(r)dr^2 - [R(r)]^2(d\theta^2 + \sin^2\theta d\varphi^2). \quad (6)$$

Equation (5) in the plane $\theta \equiv \pi/2$ yields

$$A \left(\frac{dt}{ds} \right)^2 - B \left(\frac{dr}{ds} \right)^2 - R^2 \left(\frac{d\varphi}{ds} \right)^2 = 1 \quad (7)$$

Using (2) we have integrals of motion

¹Units: $c = 8\pi G = 1$; the metric signature is $(+---)$.

$$\psi A \frac{dt}{ds} = p_0, \quad \psi R^2 \frac{d\phi}{ds} = L,$$

p_0 and L are constants.

After substitution into (7) we get

$$\psi^2 AB \left(\frac{dr}{ds} \right)^2 = p_0^2 - U_{\text{eff}}, \quad (8)$$

where the effective potential is

$$U_{\text{eff}} = A \left(\frac{L^2}{R^2} + \psi^2 \right).$$

This potential governs properties of COD. Minima of U_{eff} for fixed L correspond to SCO, maxima—to UCO. The regions where there is no minima or maxima for all L correspond to NECO. For SCO of radius r_0 we have $p_0^2 = U_{\text{eff}}$ and U_{eff} reaches minimum at $r = r_0$, i.e.,

$$U'_{\text{eff}} = \left[A' \left(\frac{L^2}{R^2} + \psi^2 \right) - \frac{2L^2 R' A}{R^3} + 2A\psi\psi' \right] = 0, \quad (9)$$

$$r = r_0.$$

Consider function

$$\tilde{L}^2(r) \equiv -\frac{R^3 \psi (A' \psi + 2A\psi')}{D}, \quad D(r) = RA'(r) - 2AR'(r). \quad (10)$$

Then condition (9) can be written as $L^2 = \tilde{L}^2(r_0)$, r_0 being a radius of a circular orbit, and $\tilde{L}^2(r_0) > 0$.

Differentiation of identity $D\tilde{L}^2 + R^3\psi(A'\psi + 2\psi') \equiv 0$ in view of (10) at the point of minimum yields

$$R^3 U''_{\text{eff}} = -D \frac{d\tilde{L}^2}{dr}, \quad r = r_0, \quad (11)$$

Thus, there are two conditions of SCO with radius r

$$\tilde{L}^2(r) > 0 \quad \text{and} \quad D(r) \frac{d\tilde{L}^2}{dr} < 0. \quad (12)$$

Obviously, the opposite signs correspond either to UCO, or NECO. This makes it convenient in the numerical search for the stability regions of circular orbits taking into account the slope of the graph $\tilde{L}^2(r)$.

III. DISTRIBUTIONS OF CIRCULAR ORBITS

Introduction of the coupling of particles with SF creates additional contributions into the Einstein equations (by means of the energy-momentum tensor) and the SF equation (by means of the source which involves the particle masses). However, we avoid this question because

we deal with the test particles moving in the external gravitational and scalar fields. This is a typical situation when the contribution of the accretion disk is negligible compared to the mass of the supermassive object at the center of an active galactic nucleus.

Under the requirements of the spherical symmetry, there is the exact static F/JNW solution of the Einstein-SF equations that describes the massless linear SF in asymptotically flat space-time outside the naked singularity. We use this solution in the form put by Virbhadra [6]

$$A(r) = \left(1 - \frac{r_s}{r} \right)^\gamma = \frac{1}{B(r)}, \quad R^2(r) = r^2 \left(1 - \frac{r_s}{r} \right)^{1-\gamma},$$

$$\phi(r) = -\frac{Q}{r_s} \ln \left(1 - \frac{r_s}{r} \right), \quad r > r_s, \quad (13)$$

where

$$r_s = 2M/\gamma, \quad \gamma = \mu/\sqrt{\mu^2 + 1}, \quad (14)$$

$M > 0$ is the mass of the system, $\mu = M/Q$, $Q \in (-\infty, \infty)$, $Q \neq 0$, is the scalar “charge”,² defined by the asymptotic dependence $\phi \sim Q/r$ for $r \rightarrow \infty$. The radial coordinate r is related to the coordinate R of [2] by $r = R + M(1 + \gamma^{-1})$. For any $Q \neq 0$ there is NS for $r = r_s$; this is the center of curvature (Schwarzschild) coordinates. There is a critical value $\gamma_{c0} = 1/2$ that separates two types of singularity at r_s ; for $\gamma \in (\gamma_{c0}, 1)$ there exists the root $r_{\text{ph}} = M(2 + 1/\gamma)$ of equation $D(r) = 0$, which is the radius of the photon sphere; it does not depend on ψ .

Investigation of [11] shows that (i) for $\gamma \in (0, \gamma_{c1})$, $\gamma_{c1} = 1/\sqrt{5}$, there is one domain of SCO with radii $r > r_s$, which covers all the space outside NS; (ii) for $\gamma \in (\gamma_{c1}, \gamma_{c0})$ there are two boundary radii $r_1^{(b)} < r_2^{(b)}$ and two rings of SCO with $r \in (r_s, r_1^{(b)})$ and $(r_2^{(b)}, \infty)$, and ring of UCO with $r \in (r_1^{(b)}, r_2^{(b)})$. (iii) For $\gamma \in (1/2, 1)$ there is a ring of NECO with radii $r \in (r_s, r_{\text{ph}})$, then the ring of UCO with radii $r \in (r_{\text{ph}}, r_1^{(b)})$, and ring of SCO with $r \in (r_1^{(b)}, \infty)$.

The boundary radii of the SCO regions can be defined by the change of the sign either of $\tilde{L}^2(r^{(L)})$ or of $d\tilde{L}^2/dr$. Correspondingly, throughout the paper we denote the roots of equations $\tilde{L}^2(r) = 0$ by index “(L)”, and the roots of $d\tilde{L}^2/dr = 0$ by index “(b)” (on condition that $\tilde{L}^2(r^{(b)}) > 0$).

In Secs. III A and III B we consider two simple examples of the interaction of particles with SF, which satisfy condition $\psi > 0$, where ψ contains an additional parameter κ describing the strength of the coupling. Therefore, we have two parameters and the problem is to find areas of

²Our notation differs from that of Chowdhury *et al.* [11], who define the scalar charge as $1/\gamma$.

these parameters in the $\gamma - \kappa$ plane and critical (bifurcation) curves that limit these areas. This is a typical problem of the catastrophe theory. There are two types of such curves.

- (a) The curves where the regions of NECO with $\tilde{L}^2(r) < 0$ appear/disappear. They correspond to simultaneous fulfillment of equations (at the same r)

$$\tilde{L}^2(r, \gamma, \kappa) = 0, \quad d\tilde{L}^2(r, \gamma, \kappa)/dr = 0. \quad (15)$$

- (b) The curves where the minima/maxima of $\tilde{L}^2(r)$ appear/disappear. They correspond to simultaneous fulfillment of equations

$$d\tilde{L}^2(r, \gamma, \kappa)/dr = 0, \quad d^2\tilde{L}^2(r, \gamma, \kappa)/dr^2 = 0. \quad (16)$$

However, in the numerical treatment it is more convenient to apply a straightforward determination of roots of $\tilde{L}^2(r)$ and $d\tilde{L}^2(r)/dr$. For admissible parameter values³ we look for possible $r^{(L)}(\gamma, \kappa)$ and $r^{(b)}(\gamma, \kappa)$ and control the fulfillment of conditions (12) for SCO and analogous conditions for UCO and NECO for orbits with radii r between these values. Namely, for fixed γ, κ we test the existence of the solutions for $r > r_s$: $\tilde{L}^2(r) = 0$ and/or $d\tilde{L}^2/dr = 0$, which separate r corresponding to SCO, UCO and NECO. The emergence and disappearance of these solutions for some values of γ, κ occurs on the bifurcation curves separating the regions with different CODs in $\gamma - \kappa$ plane, colored in different colors in the Figs. 2, 3, 4 below. The existence of different intervals for admissible radii of SCO and UCO is correspondingly shown in Tables I and II (see below).

A. Power-law coupling

As mentioned above, we have no considerations other than the simplicity criterion regarding the choice of $\psi(\phi)$ to formulate modifications of the relativistic gravity theory. The only restrictions must be imposed by known weak-field experiments, which can be satisfied by an appropriate choice of model parameters that regulate the strength of the interaction, not excluding qualitative effects near the naked singularity. In this situation, we will restrict ourselves to the “toy” examples of the power-law coupling (this subsection) and exponential coupling (Sec. III B), which seem to be the simplest.

In the case of the power-law coupling

$$\psi(\phi) = 1 + \kappa\phi^{2n}, \quad n = 1, 2, \dots \quad (17)$$

where we consider the even powers of ϕ in (17) and we put $\kappa > 0$ so as to have $\psi(\phi) > 0$ for all ϕ .

³In fact, in case of both couplings (17), (20) we tested the values of $|\kappa| \in [0, 10)$, but the region of $|\kappa| > 1$ does not result in qualitatively new elements and it is not shown in figures.

From (10) we have

$$\tilde{L}^2(r) = \frac{r_s r (1 - r_s/r)^{1-\gamma} \psi F(r, Q, n)}{2(1 - r_{\text{ph}}/r)},$$

$$F(r) = \gamma + \kappa \left[\gamma \phi^{2n} - \frac{2n\gamma}{\mu} \phi^{2n-1} \right]. \quad (18)$$

Without loss of the generality, we assume $Q > 0$.

We begin with some general analytical results concerning the sign of $\tilde{L}^2(r)$ (i.e., where either SCO or UCO can exist) that follow directly from (18).

For a sufficiently large r we have $\tilde{L}^2(r) \approx rM$ and the conditions (12) are fulfilled; therefore there is always an unbounded outer region of SCO, which includes the nonrelativistic orbits.

Now we proceed to the singularity neighborhood. For $r \rightarrow r_s$ we have $F(r) > 0$. Therefore, $\tilde{L}^2(r) > 0$ is increasing at least in small vicinity of r_s for $\gamma \in (0, 1/2)$ (SCO) and there is NECO for $\gamma \in (1/2, 1)$.

There is bifurcation value $\kappa = \kappa_{cr}$,

$$\kappa_{cr} = \frac{\mu^{2n}}{(2n-1)^{2n-1}} = \frac{1}{(2n-1)^{2n-1}} \left(\frac{\gamma^2}{1-\gamma^2} \right)^n, \quad (19)$$

where the minimum of $F(r)$ changes its sign from positive for $\kappa \in (0, \kappa_{cr})$ to negative for $\kappa > \kappa_{cr}$. This is the only minimum of $F(r)$, therefore for $\kappa > \kappa_{cr}$ we have only two zeros of this function, which disappear at κ_{cr} . Equation (19) yields the bifurcation curve in the $\gamma - \kappa$ plane corresponding to (15).

The following cases of behavior of $\tilde{L}^2(r)$ are possible.

- (i) For $0 < \kappa < \kappa_{cr}$ and $\gamma \in (0, 1/2)$ we have $\tilde{L}^2(r) > 0$ for all r ;
- (ii) For $0 < \kappa < \kappa_{cr}$ and $\gamma \in (1/2, 1)$ there are no circular orbits under the photon sphere and $\tilde{L}^2(r) > 0$ for $r > r_{\text{ph}}$;
- (iii) For $\kappa > \kappa_{cr}$ there are only two points $r_1^{(L)}, r_2^{(L)}$, where $F(r)$ changes its sign. Therefore, for $\gamma \in (0, 1/2)$ we have $\tilde{L}^2(r) < 0$ in $(r_1^{(L)}, r_2^{(L)})$ (NECO) and $\tilde{L}^2(r) > 0$ otherwise.
- (iv) For $\kappa > \kappa_{cr}$ and $\gamma \in (1/2, 1)$ the results depend upon mutual disposition of $r_1^{(L)}, r_2^{(L)}, r_{\text{ph}}$.

For $n = 1$ the points $r_1^{(L)}, r_2^{(L)}$ can be easily found:

$$r_{1,2}^{(L)} = \frac{r_s}{1 - e^{-\xi_{\pm}}}, \quad \xi_{\pm} = \frac{2}{\gamma} \left(1 \pm \sqrt{1 - \frac{\mu^2}{\kappa}} \right), \quad \kappa > \mu^2.$$

We studied numerically function $\tilde{L}^2(r)$ for $n = 1, 2$. Figure 2 shows areas with qualitatively different COD in $\gamma - \kappa$ plane which correspond Table I. Here we confined ourselves with $0 \leq \kappa \leq 1$, which is sufficient to see the general tendency of the results. The areas of Fig. 2 with qualitatively different SOD are colored in different colors

TABLE I. Possible SCO and UCO regions for monomial coupling (17) in correspondence to different areas of Fig. 2.

N	SCO	UCO	sign($\gamma - 0.5$)
1	$(r_1^{(b)}, \infty)$	$(r_{\text{ph}}, r_1^{(b)})$	+
2	(r_s, ∞)	...	-
3	$(r_s, r_1^{(b)}) \cup (r_2^{(b)}, \infty)$	$(r_1^{(b)}, r_2^{(b)})$	-
4	$(r_2^{(L)}, \infty)$	$(r_{\text{ph}}, r_1^{(L)})$	+
5	$(r_1^{(L)}, \infty)$...	+/-
6	$(r_2^{(b)}, r_3^{(L)}) \cup (r_4^{(b)}, \infty)$	$(r_1^{(L)}, r_2^{(b)}) \cup (r_{\text{ph}}, r_4^{(b)})$	+
7	$(r_s, r_1^{(b)}) \cup (r_3^{(L)}, \infty)$	$(r_1^{(b)}, r_2^{(L)})$	-
8	$(r_s, r_1^{(b)}) \cup (r_2^{(b)}, r_3^{(b)}) \cup (r_4^{(b)}, \infty)$	$(r_1^{(b)}, r_2^{(b)}) \cup (r_3^{(b)}, r_4^{(b)})$	-
9	$(r_s, r_1^{(b)}) \cup (r_3^{(L)}, r_4^{(b)}) \cup (r_5^{(b)}, \infty)$	$(r_1^{(b)}, r_2^{(L)}) \cup (r_4^{(b)}, r_5^{(b)})$	-
10	$(r_2^{(b)}, r_3^{(L)}) \cup (r_4^{(b)}, \infty)$	$(r_1^{(L)}, r_2^{(b)}) \cup (r_{\text{ph}}, r_4^{(b)})$	+
11	$(r_2^{(b)}, r_3^{(b)}) \cup (r_4^{(L)}, r_5^{(b)}) \cup (r_6^{(b)}, \infty)$	$(r_1^{(L)}, r_2^{(b)}) \cup (r_3^{(b)}, r_{\text{ph}}) \cup (r_5^{(b)}, r_6^{(b)})$	+
12	$(r_3^{(b)}, r_4^{(b)}) \cup (r_4^{(L)}, \infty)$	$(r_1^{(L)}, r_2^{(b)}) \cup (r_3^{(b)}, r_{\text{ph}})$	+
13	$(r_2^{(L)}, \infty)$	$(r_1^{(L)}, r_{\text{ph}})$	+

indicated in the legend of each of two panels with the number associated with certain row of the Table I. Every row shows intervals of the radii of possible SCO and UCO regions, in accordance with the indexing introduced above).

As an example, we explain the notations in case of the orange area (number 9 of the legend) in the right panel ($n = 2$) of Fig. 2. Correspondingly, row 9 of Table I shows that there exist boundary radii $r_1^{(b)}, r_2^{(L)}, r_3^{(L)}, r_4^{(b)}, r_5^{(b)}$ of regions with different stability properties (in ascending order of the lower indexes), which of course depend on γ and κ inside the orange area. Here the coordinate r_s of the singularity is also involved. The left column (row 9) shows that for every γ and κ of this area, there exist such values of boundary radii that function $\tilde{L}^2(r) > 0$ is increasing in

three intervals $(r_s, r_1^{(b)}), (r_3^{(L)}, r_4^{(b)}), (r_5^{(b)}, \infty)$, where we have SCO (see Fig. 1, left panel). This function decreases in $(r_1^{(b)}, r_2^{(L)})$ and $(r_4^{(b)}, r_5^{(b)})$ (see row 9, middle column of Table I, UCO). In the remaining intervals, not explicitly shown in Table I, we have NECO. The right column indicates that $\gamma < 1/2$, i.e., the orange region is to the left of the vertical dashed line in the right panel of Fig. 2.

Figure 1 (right panel) shows the other example of the graph of $\tilde{L}^2(r)$, which is related to row 11 of Table I (brown region in the right panel of Fig. 2, to the right of the dashed line $\gamma = 1/2$).

The case $\gamma = 1/2$ is poorly visible in the figures and we describe it separately. In this case $D(r) < 0$ for all $r > r_s$.

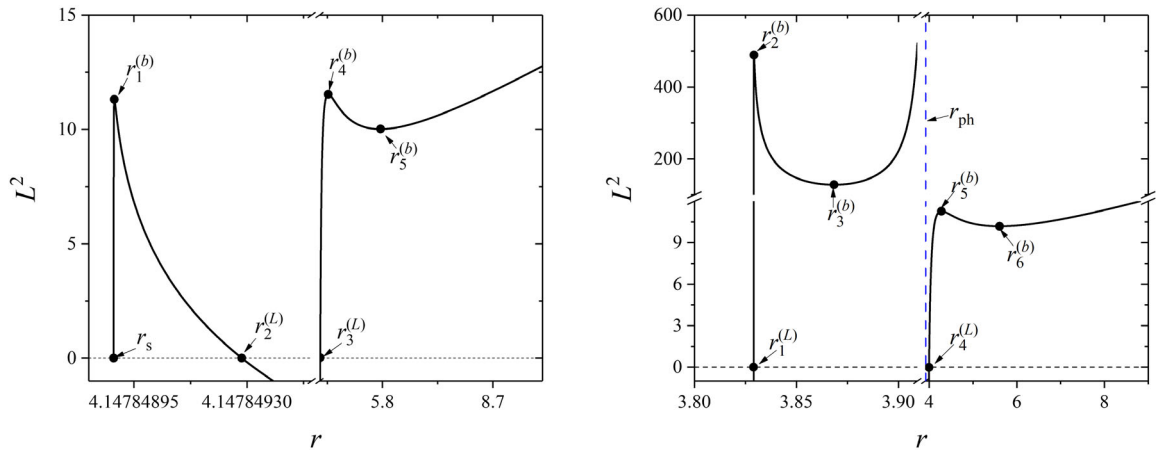


FIG. 1. Typical behavior of L^2 for area 9 (left) and area 11 (right) of the Table I and Fig. 2 in case of monomial coupling (17). There is very fast growth of L^2 and very small size of the SCO regions near the singularity. For case 9: $r_1^{(b)} - r_s \simeq 2 \times 10^{-9}$; for case 11: $r_2^{(b)} - r_1^{(L)} \simeq 0.0001$.

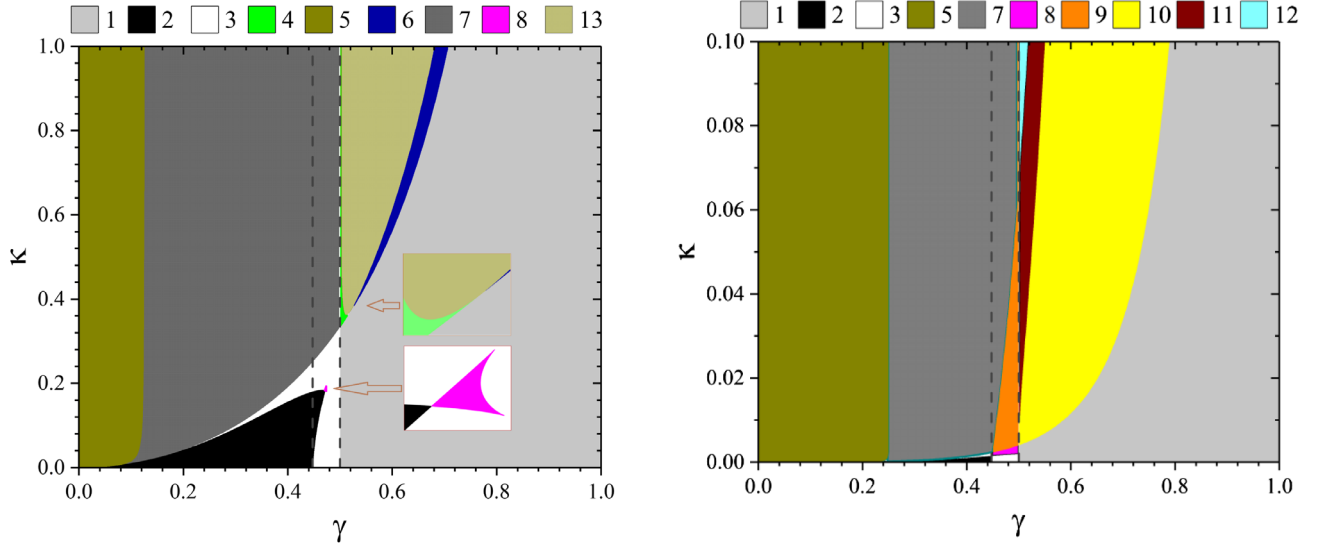


FIG. 2. Possible COD cases for the coupling (17). Left panel: $n = 1$; Right panel: $n = 2$. The dashed vertical lines correspond to critical values of $\gamma_{c0} = 1/2$ and $\gamma_{c1} = 1/\sqrt{5}$. The rectangles in the left panel represent enlarged elements, shown by the arrows.

For $n = 1$, there is a critical value $\kappa_{cr} \approx 0.33$ such that for $\kappa < \kappa_{cr} \exists r_1^{(b)}$ such that $\tilde{L}^2(r) > 0$ decreases for $r \in (r_{ph}, r_1^{(b)})$ corresponding to UCO region near the center, and increases for $r > r_1^{(b)}$ (SCO). Here $r_1^{(b)}$ is the point of minimum of \tilde{L}^2 ; this minimum decreases as κ grows and becomes negative after $\kappa > \kappa_{cr}$, when $\exists r_1^{(L)}, r_2^{(L)}$ such that there is UCO region with radii $r \in (r_{ph}, r_1^{(L)})$, NECO for $r \in (r_1^{(L)}, r_2^{(L)})$, and SCO for $r > r_2^{(L)}$.

In the case $\gamma = 1/2$, $n = 2$, we have an analogous situation; the critical κ_{cr} can be found from (19).

B. Exponential coupling

Here we consider an exponential type of the coupling, inspired by considerations from [27,29] in the form of

$$\psi(\phi) = e^{\kappa\phi^n}; \quad \xi = e^{\kappa\phi^n} - 1, \quad n = 1, 2, \dots, \quad (20)$$

now $\psi(\phi) > 0$ for all values of ϕ and $\kappa \in (-\infty, \infty)$. Note that unlike Sec. III A, the sign of Q is significant for odd n , however, in this case instead of considering negative Q one can change $\kappa \rightarrow -\kappa$; therefore, we always assume $Q > 0$ and correspondingly $\phi > 0$.

We have from (10)

$$\tilde{L}^2 = rM \frac{(1 - r_s/r)^{1-\gamma}}{1 - r_{ph}/r} \left(1 - \frac{\kappa n}{\mu} \phi^{n-1} \right) e^{2\kappa\phi^n}. \quad (21)$$

For $\kappa < 0$ we always have $\tilde{L}^2 > 0$ for $r > r_{ph}$, if $\gamma \in (1/2, 1)$ and NECO for $r_s < r < r_{ph}$; and $\tilde{L}^2 > 0, \forall r > r_s$ if $\gamma \in (0, 1/2)$.

For $n > 1$ and $\kappa > 0$, the root of equation $\tilde{L}^2 = 0$ can be written as

$$r^{(L)} = \frac{1}{1 - e^{-\xi}}, \quad \xi = 2 \left(\frac{\gamma}{\kappa n} \right)^{1/(n-1)} \left[\frac{1}{\sqrt{1 - \gamma^2}} \right]^{n/(n-1)} > 0.$$

These roots are always uniquely defined, no appearance/disappearance of roots occurs. Therefore, there are no bifurcation curves of type (a) [see (15)].

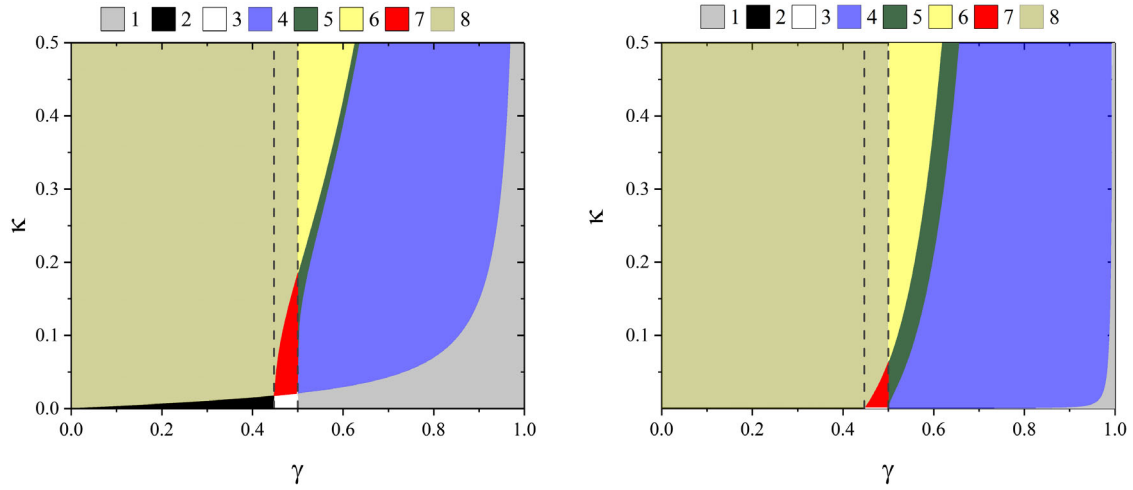
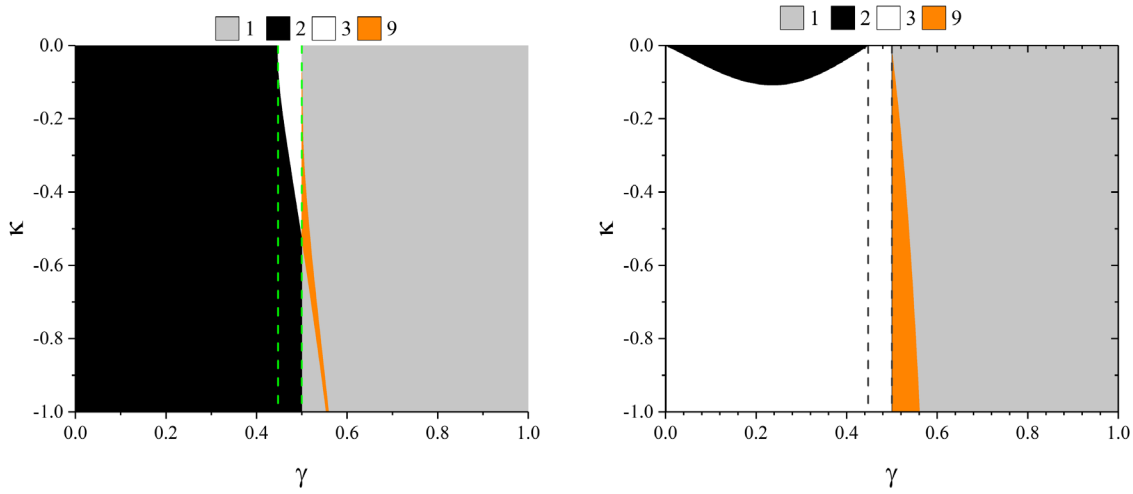
Further information on COD obtained numerically is represented in Figs. 3, 4 and Table II. The latter contains one more column indicating the possible sign of κ .

In case of $n = 1$ a detailed analytic treatment is possible. There is an obvious bifurcation curve

$$\kappa_{b,0} = \mu = \gamma / \sqrt{1 - \gamma^2},$$

that separates regions in the $\gamma - \kappa$ plane:

- (i) For $\kappa < \mu, \gamma \in (0, 1/2)$ we always have $\tilde{L}^2 > 0, \forall r > r_s$.
- (ii) For $\gamma \in (1/2, 1)$ we have $\tilde{L}^2 > 0$ (UCO or SCO) for $r > r_{ph}$ and NECO for $r_s < r < r_{ph}$.
- (iii) There is a reverse situation for $\kappa > \mu$. In particular, there is no circular orbits at all for $\gamma \in (0, 1/2)$; in this case the repulsion of particles from the center due to SF overcomes usual gravitational attraction. For $\gamma \in (1/2, 1)$ we have $\tilde{L}^2 > 0$ for $r < r_{ph}$. There is SCO for $r \in (r_s, r_1^{(b)})$, UCO for $r \in (r_1^{(b)}, r_{ph})$ and NECO for $r > r_{ph}$. The situations with NECO for large r are obviously unphysical.
- (iv) From the conditions (9), (11) we obtain analytic expression for two boundary radii


 FIG. 3. Possible COD cases for (20), $\kappa > 0$. Left panel: $n = 2$; Right panel: $n = 4$. The dashed vertical lines as in Fig. 2.

 FIG. 4. Possible COD cases for (20), $\kappa < 0$. Left panel: $n = 2$; Right panel: $n = 4$. The dashed vertical lines as in Fig. 2.

$$r_{1,2}^{(b)} = \gamma^{-1} \left[1 + 3\gamma + \sqrt{1 - \gamma^2 \kappa} \right. \\ \left. \pm \sqrt{\gamma^2(5 - \kappa^2) + 2\sqrt{1 - \gamma^2 \kappa} + \kappa^2 - 1} \right]. \quad (22)$$

These roots disappear on the type (b) bifurcation curve [see (16)] with branches

$$\kappa_{1,2} = \frac{\gamma \pm \sqrt{1 - 4\gamma^2}}{\sqrt{1 - \gamma^2}} = \mu \pm 1, \quad \gamma < \frac{1}{2}. \quad (23)$$

TABLE II. Possible SCO and UCO regions for the exponential coupling (20) in correspondence with different areas of Figs. 3, 4.

N	SCO	UCO	sign(κ)	sign($\gamma - 0.5$)
1	$(r_1^{(b)}, \infty)$	$(r_{\text{ph}}, r_1^{(b)})$	+/-	+
2	(r_s, ∞)	...	+/-	-
3	$(r_s, r_1^{(b)}) \cup (r_2^{(b)}, \infty)$	$(r_2^{(b)}, r_3^{(b)})$	+/-	-
4	$(r_s, r_1^{(L)}) \cup (r_2^{(b)}, \infty)$	$(r_{\text{ph}}, r_2^{(b)})$	+	+
5	$(r_s, r_1^{(b)}) \cup (r_2^{(L)}, r_3^{(b)}) \cup (r_4^{(b)}, \infty)$	$(r_1^{(b)}, r_{\text{ph}}) \cup (r_3^{(b)}, r_4^{(b)})$	+	+
6	$(r_s, r_1^{(b)}) \cup (r_2^{(L)}, \infty)$	$(r_1^{(b)}, r_{\text{ph}})$	+	+
7	$(r_1^{(L)}, r_2^{(b)}) \cup (r_3^{(b)}, \infty)$	$(r_2^{(b)}, r_3^{(b)})$	+	-
8	$(r_1^{(L)}, \infty)$...	+	-
9	$(r_1^{(b)}, r_2^{(b)}) \cup (r_3^{(b)}, \infty)$	$(r_{\text{ph}}, r_1^{(b)}) \cup (r_2^{(b)}, r_3^{(b)})$	-	-

If we include into consideration the negative γ and κ , these branches form the closed curve in the $\gamma - \kappa$ plane, which cross the γ -axis at $\gamma = \pm 1/\sqrt{5}$.

IV. DISCUSSION

We have shown that introduction of the coupling of particles with SF can essentially change the SCO distribution around the naked singularity described by the F/JNW solution and creates a wealth of new types. In particular, COD with three SCO regions appear in case of the nontrivial coupling, which are absent in case of F/JNW. Namely, in case the geodesic motion ($\kappa = 0$), when the test particles move along geodesics in the F/JNW metric, we have only one case of disjoint SCO regions. In case of the monomial coupling (17), we found areas in the $\gamma - \kappa$ plane corresponding to three SCO regions (see lines 8, 9 and 11) of Table I, which are separated by UCO/NECO rings. In case of the exponential coupling analogous case corresponds to line 5 of Table II.

Let us briefly discuss possible applications of the obtained results to astrophysical objects.

The relation of the SCO distributions to the accretion disks around compact objects is straightforward in the Page-Thorn model [31]. Moreover, one can expect that main signatures of the SCO rings, separated by the instability regions, will retain their relevance in more complex models of accretion disks as well. For example, the dark spot at the center of an accretion disk around a black hole is ultimately associated with the NECO and UCO regions, although the underlying physical processes in the disk can be very complex. Thus, if the configurations with SF really exist, then the disconnected structure of the SCO distributions may be an important feature that can be related to the observational properties of the accretion discs in astrophysical systems.

However, the occurrence of the most interesting COD structures require a fine tuning, because they occupy rather small areas in the $\gamma - \kappa$ plane. Also, it is evident that the existence of such fine details is possible in the region of strong gravitational field that is not far from the singularity, where the “unusual” annular structures are typically very small and they might be difficult to observe.

Are there restrictions of the weak-field gravitational experiments in connection with the above results? The Post-Newtonian approximation of the metric (13) in the isotropic coordinates does not involve the scalar charge Q , so the PPN-parameters of F/JNW solution are the same as in the Schwarzschild case [32]. Therefore, if there is no interaction of particles with SF, then in the case when the values of M and Q are of the same order, the latter practically is not restricted by the Solar system gravitational experiments.

The situation changes, if the interaction is switched on. The post-Newtonian analysis can be easily carried out thanks to the fact that the Eq. (2) can be considered as the geodesics in the space-time with the conformal metric $\tilde{g}_{\mu\nu} = \psi^2 g_{\mu\nu}$ ($\psi > 0$). In the cases described by (17) and (20), for $|\xi| \ll 1$, we have $\xi \sim \kappa|\phi|^n \sim \kappa(|Q|/r)^n$.

For both models (17) and (20), the constant κ should be considered universal. Then, if $n = 1$ in the case of (17) or $n = 1, 2$ in the case of (20), for $\kappa \sim 1$ the Solar system experiments put rather strong restrictions on the scalar charge of the system. Otherwise, one must consider $\kappa \ll 1$ and the properties of SCO distributions will be essentially the same as for $\kappa = 0$, even if Q is considerable. There seems to be nothing unusual about the images of accretion disks around M87* and SgrA* provided by the Event Horizon Telescope (EHT) team [33,34]. Therefore, it may seem that the case of significant Q in these systems with $\kappa \sim 1$ can be excluded. However, it should be kept in mind that the current resolution of EHT may be insufficient to resolve the discussed above (putative) fine structure of the accretion discs (cf. [35]). Also, the absence of such structures in M87* and SgrA* does not mean that they cannot be present in other objects.

For larger n and $\kappa \sim 1$, the scalar charge does not contribute into the post-Newtonian orders and therefore, to the PPN-parameters; then the Solar system experiments do not restrict Q and κ . In this case we have a sufficient freedom to choose Q and κ .

Although F/JNW is a very special solution dealing with massless linear SF, one can suppose that situation with several nonconnected SCO regions represents more general case. For example, it was pointed out in [24] that the circular orbits for static spherically symmetric configurations with the SF potential $\sim \phi^{2p}$, $p > 2$, have much in common with the F/JNW case. We expect that the appearance of new COD types after switching on the coupling of particles with SF occurs in this case as well.

ACKNOWLEDGMENTS

The authors express their sincere gratitude to all those who support Ukraine in the fight against the aggression of the Russian Federation. We are grateful to the anonymous referee for helpful comments, which stimulated the improvement of the manuscript. O. S. S. is thankful to Horst Stöcker for the warm hospitality at Frankfurt Institute for Advanced Studies. This work has been supported in part by the scientific program “Astronomy and space physics” of Taras Shevchenko National University of Kyiv, Project No. 22БФ023-01.

- [1] I. Z. Fisher, *Zh. Exp. Theor. Phys.* **18**, 636 (1948), [arXiv: gr-qc/9911008](#).
- [2] A. I. Janis, E. T. Newman, and J. Winicour, *Phys. Rev. Lett.* **20**, 878 (1968).
- [3] M. Wyman, *Phys. Rev. D* **24**, 839 (1981).
- [4] A. G. Agnese and M. La Camera, *Phys. Rev. D* **31**, 1280 (1985).
- [5] M. D. Roberts, *Astrophys. Space Sci.* **200**, 331 (1993).
- [6] K. S. Virbhadra, *Int. J. Mod. Phys. A* **12**, 4831 (1997).
- [7] S. Abdolrahimi and A. A. Shoom, *Phys. Rev. D* **81**, 024035 (2010).
- [8] K. S. Virbhadra, S. Jhingan, and P. S. Joshi, *Int. J. Mod. Phys. D* **6**, 357 (1997).
- [9] B. C. Xanthopoulos and T. Zannias, *Phys. Rev. D* **40**, 2564 (1989).
- [10] V. I. Zhdanov and O. S. Stashko, *Phys. Rev. D* **101**, 064064 (2020).
- [11] A. N. Chowdhury, M. Patil, D. Malafarina, and P. S. Joshi, *Phys. Rev. D* **85**, 104031 (2012).
- [12] G. Gylchev, P. Nedkova, T. Vetsov, and S. Yazadjiev, *Phys. Rev. D* **100**, 024055 (2019).
- [13] G. Gylchev, J. Kunz, P. Nedkova, T. Vetsov, and S. Yazadjiev, *Eur. Phys. J. C* **80**, 1017 (2020).
- [14] D. Pugliese, H. Quevedo, and R. Ruffini, *Phys. Rev. D* **83**, 024021 (2011).
- [15] D. Pugliese, H. Quevedo, and R. Ruffini, *Phys. Rev. D* **88**, 024042 (2013).
- [16] R. S. Vieira, J. Schee, W. Kluźniak, Z. Stuchlík, and M. Abramowicz, *Phys. Rev. D* **90**, 024035 (2014).
- [17] Z. Meliani, F. H. Vincent, P. Grandclément, E. Gourgoulhon, R. Monceau-Baroux, and O. Straub, *Classical Quantum Gravity* **32**, 235022 (2015).
- [18] Z. Stuchlík and J. Schee, *Int. J. Mod. Phys. D* **24**, 1550020 (2015).
- [19] O. S. Stashko and V. I. Zhdanov, *Gen. Relativ. Gravit.* **50**, 105 (2018).
- [20] Z. Stuchlík, J. Schee, and D. Ovchinnikov, *Astrophys. J.* **887**, 145 (2019).
- [21] I. Dymnikova and A. Poszwa, *Classical Quantum Gravity* **36**, 105002 (2019).
- [22] P. Slaný and Z. Stuchlík, *Eur. Phys. J. C* **80**, 587 (2020).
- [23] O. Stashko and V. Zhdanov, *Ukr. J. Phys.* **64**, 189 (2019).
- [24] O. S. Stashko, V. I. Zhdanov, and A. N. Alexandrov, *Phys. Rev. D* **104**, 104055 (2021).
- [25] C. Brans and R. H. Dicke, *Phys. Rev.* **124**, 925 (1961).
- [26] T. Damour and G. Esposito-Farese, *Classical Quantum Gravity* **9**, 2093 (1992).
- [27] T. Damour and G. Esposito-Farese, *Phys. Rev. Lett.* **70**, 2220 (1993).
- [28] A. De Felice and S. Tsujikawa, *Living Rev. Relativity* **13**, 3 (2010).
- [29] Y. Shtanov, *Phys. Lett. B* **820**, 136469 (2021).
- [30] C. M. Will, *Living Rev. Relativity* **17**, 4 (2014).
- [31] D. N. Page and K. S. Thorne, *Astrophys. J.* **191**, 499 (1974).
- [32] J. B. Formiga, *Phys. Rev. D* **83**, 087502 (2011).
- [33] The Event Horizon Telescope Collaboration, *Astrophys. J. Lett.* **875**, L1 (2019).
- [34] The Event Horizon Telescope Collaboration, *Astrophys. J. Lett.* **930**, L12 (2022).
- [35] M. Miyoshi, Y. Kato, and J. Makino, *Astrophys. J.* **933**, 36 (2022).